Rotating Hub Drag Prediction Methodology

Matthew J. Hill
Senior Engineer
mjhill@bellhelicopter.textron.com

Matthew E. Louis
Engineer
mlouis01@bellhelicopter.textron.com

Bell Helicopter Textron Inc.
Fort Worth, TX

Hub drag reduction has long been a sought after technology goal. This is because modern rotary-wing hubs can account for up to 30% of the drag of an aircraft. However, achieving realizable benefits on production aircraft requires a significant demonstrable improvement in present design and analysis tools. Bell Helicopter is currently engaged in a four year NRTC/CRI project with one of the principal criteria for success being the identification of a physics-based analysis methodology capable of accurately predicting drag on realistic hub geometries. The results from the fourth and final year of the project are described herein and concern the applications to rotating hubs. Details offered include a description of a recent Bell aircraft wind tunnel test used for correlation, the grid generation paradigm used, and the correlation between measured and computed data for both pitch and yaw orientations, and future work planned.

INTRODUCTION

Modern rotary-wing hubs can account for up to 30% of the drag of the aircraft (Ref. 1). Hub drag reduction has been a long sought after technology goal. Given the ever increasing cost of wind tunnel testing, particularly the numerous configurations that may need to be tested to identify a usable hub drag reduction concept, achieving realizable benefits on production aircraft requires a significant and demonstrable improvement in the design and analysis tools and methodology used for such investigations.

Computational fluid dynamics (CFD) methods have a ubiquitous presence in current analysis and design processes for modern rotorcraft. The majority of the analysis approaches employ traditional structured overset gridding that require significant setup time in generating individual grids around component parts. This process is particularly cumbersome for complex geometries like rotor hubs. Unstructured grid methods offer the ability to reduce the significant pre-processing time associated with component grid generation. Entire aircraft configurations can be effectively meshed in days instead of months. These methods are uniquely adept at treating the complexities of realistic rotor hub geometries.

The general technical approach taken in the present work was to identify an unstructured Navier-Stokes solver capable of predicting the drag (and other aerodynamic characteristics) of realistic and complex hub configurations representative of current helicopters. Unstructured grid methods are being developed that significantly reduce the pre-processing time associated with grid generation and are uniquely adept at treating the complexities of a realistic rotor hub geometry. Bell Helicopter has significant experience in the application of the CFD solver U^2NCLE (Ref. 2-3) to complex configurations and it has been applied to the analysis of static hub configurations (Ref. 4-5). However, for the analysis of rotating hub configurations the NASA unstructured flow solver FUN3D (Ref. 6) is used. FUN3D has been used in previous rotorcraft CFD analysis (Ref. 7) and includes the capability to use moving overset meshes, which are well suited to the analysis of bodies in relative motion. Overset grid capability is provided by the DiRTlib (Ref. 8) and SUGGAR++ (Ref. 9) software libraries.

There are a variety of wind tunnel data sets involving both non-rotating and rotating hub configurations that are suitable for validation. Perhaps the most comprehensive series of wind

Presented at the American Helicopter Society Specialists' Conference on Future Vertical Lift Aircraft Design, January 18-20 2012.

tunnel investigations were performed by NASA (Refs. 10–18). Numerous tests were conducted to examine the effects on drag of a variety of hub and pylon fairings. Several tests were conducted on a Sikorsky XH-59A (Refs. 10–16), with both single and co-axial hubs (non-rotating). Another test involved a rotating hub geometry on a Bell Helicopter 0.20-scale Model 222 (Refs. 17-18) force and moment model.

It was deemed that the most appropriate data set involved a modern Bell Helicopter aircraft recently tested in a model build-up with a significant amount of data available for a realistic hub configuration. This test provided significant data for correlation, evaluation, and selection of a suitable analytical tool in the present work. The computation of and correlation with the aforementioned Bell Helicopter test data obtained during the first two years of the project have been summarized by Bridgeman et al. (Ref. 4-5). In 2011, the final year of the project, a new wind tunnel test was performed that included a rotating hub configuration and several additional static configurations.

To date, very little has been reported in the open literature on computational predictions of hub drag, including correlations with measured data. This has largely been due to the intensive efforts required to generate a high quality mesh that models a complex hub, the state of development of unstructured solvers, and the availability of test data. Wake et al (Ref. 19) used the commercial code FLUENT to predict the hub drag and drag reduction of several hub and intermediate fairing shapes, and obtained good correlation with measured data from the NASA XH-59A tests (Refs. 10-16) and tests performed as part of their investigation. However, the geometries used in the computational models were relatively simple compared with real-world hubs. As part of a drag reduction investigation, Le Chuiton et al (Ref. 20) applied both structured overset and unstructured methods to a fairly complex representation of a non-rotating EC145 hub. The computations were only performed at one pitch (+10 deg) and yaw (0 deg) orientation. The structured solver demonstrated very good correlation (within 7.5% of experimental drag) with test data, but the unstructured solver, which was still in development, could only get within about 30% of the experimental drag. Bridgeman et al. (Ref. 4-5) achieved hub drag predictions to within 5% using the U^2NCLE solver for a pitch sweep. However, some simplifications were made to the hub geometry model. Shenoy et al. (Ref. 21) examined and deconstructed the sources of hub drag on a moderately complex model at model and full scales.

The present paper is organized as follows. First, the wind tunnel test data is reported. Next, the computational methodology and grid generation paradigm is presented. The correlation between measured and computed data for both pitch and yaw orientations is then reported. Finally, the preliminary results of a computational experiment into notional hub drag reduction designs are discussed.

WIND TUNNEL TEST DATA

In 2011, a new wind tunnel test was conducted on the same scale model of a modern Bell Helicopter light twin aircraft that was reported by Bridgeman (Ref. 4-5). This test was repeated at the 2-m × 3-m low-speed wind tunnel at the National Research Council (NRC) of Canada in Ottawa. The facility is a vertical, single-return, closed circuit tunnel with a rectangular cross-section (2-m × 3-m) and driven by a 2000 hp electric motor connected to a four-bladed fan. The empty section tunnel is capable of producing wind speeds of up to 140 m/sec at atmospheric static pressure.

In the new test, the static hub model was replaced with a rotating model hub, which is shown in Figure 1. Pitch and yaw sweeps were conducted for both static and rotating hub configurations. Transition strips were used at several locations on the model, a standard image system was used for tares and interference (single support strut mount), and wind tunnel wall corrections were made to the measured data. Force and moment data is time-averaged for all runs.

The force and moment data are used to identify the aerodynamic characteristics of the isolated fuselage (IF) and the fuselage plus hub (FH) configurations. Hub drag has been defined by Bridgeman as the zero lift drag differential between these two configurations for a non-rotating hub.

Figure 2 shows the wind tunnel results from the pitch sweep. As can be seen in the figure, the static and rotating hub results are nearly indistinguishable between each other.

COMPUTATIONAL METHODOLOGY

The flow solver used in this work is FUN3D. FUN3D is an unstructured, finite-volume Reynolds-averaged Navier-Stokes (RANS) flow solver from the NASA Langley Research Center. It is a node-centered code that supports mixed-element (tetrahedral, pyramids, prism) meshes. It supports rigid, deforming, and overset mesh-motion options. The overset capability is provided by DiRTlib and SUGGAR++.

All computations were performed at the tunnel conditions of 150 kn and sea-level resulting in the

flow parameters M_∞=0.2264 and Re_∞ = 11.25 x10^6 for the 20% model scale length of 88.2 inches. The Spalart-Allmaras (Ref. 22) turbulence model is used for all computations. All computations were performed on Bell Helicopter's computational cluster Nemo. Nemo is a 43 node Linux cluster. Each node has twelve Intel 2.67 GHz processors with 4 GB memory per core.

All rotating hub cases were initialized from static hub steady solutions. For the unsteady rotating hub cases, time advancement is carried out with a modified second-order backward difference dual-time scheme (Ref 23-24). The standard time step corresponds to a 0.9 degrees change in hub azimuth per time step. The time step size was selected based on the hub rotation speed and a characteristic period of one-fourth of a hub rotation (four-blade hub). One hundred time steps were used for one characteristic period (400 time steps per full rotation). Time advancement is performed under the guidance of a temporal error controller (Ref. 7,23) in which dual time subiterations are carried out within each time step until either the L_2-norm of the nonlinear residual is reduced to a specified fraction of the estimated error, or a specified maximum number of subiterations have been performed. For all results shown here, an error fraction of 0.01 is used and the maximum number of subiterations allowed is 50.

Rigid, overset body motion is used for the rotating hub simulations. The rotating hub motion is also treated as being periodic in time. This allows the domain connectivity information (DCI) files generated by SUGGAR++ to be reused after the first revolution. One DCI file is needed for each time step. The angle of attack and yaw settings in FUN3D only control flow direction and do affect grid orientation. Therefore, the DCI files only need to be generated once for a given hub configuration. The DCI files can be reused between different pitch and yaw angles.

Grid Generation

The grid generation paradigm used in this work largely follows the current methodology used at Bell Helicopter as detailed by Bridgeman et al. (Ref. 4-5). A CATIA model for the aircraft wind tunnel configuration is directly imported into ICEM CFD (Ref. 24). An outer boundary surface (typically a sphere with a radius of 25 vehicle lengths) is defined. Material (flow) point and orphan (model interior) points are then defined in ICEM. The model topology is additionally defined by extracting the defining curves, which are automatically created at the edges of the embedded surfaces and naturally at sharp corners. Grid resolution is almost entirely controlled by defining the maximum and minimum sizes for the triangles on each surface or group of surfaces. Final control is achieved by setting an associated maximum deviation which is defined as the distance between the triangle midpoint and the actual CAD surface. This allows for control of the resolution in regions of high curvature.

ICEM then generates an octree tetrahedral mesh. The obtained surface resolution is examined, spacing controls modified as required, and the process repeated. After a suitable first pass surface is obtained, the mesh is checked for numerous errors using internal tools, and fixes completed as necessary. The tetrahedral grid is then smoothed several times based on aspect ratio and re-examined each time. A final Laplace smoothing is performed on the surface mesh and the resultant volume mesh is written out to a formatted UGRID file.

The mixed element volume mesh generation is initiated by reading the UGRID file into SOLIDMESH (Ref. 26) using the extract surface option. This discards the volume mesh created by ICEM and leaves the body and outer boundary triangulated surface meshes. The outer boundary patch is set to no prismatic growth, the Reynolds number and reference length are defined, and the *y+* value is set to a value of one. A script file is written by SOLIDMESH that is executed by AFLR3 (Ref. 27-28). AFLR3 generates the mixed element volume mesh. Other than model specific inputs, all default parameters in AFLR3 are used.

The generation of an overset grid system requires a few additional steps within this methodology, mostly in ICEM. The first step is to separate the rotating and non-rotating body surfaces. This was accomplished by modifying the fuselage in the region of the hub and creating a "hub well" region for the hub to rotate within. The size of the well was set to allow sufficient grid overlap between the two grids. Figure 3 compares the overset and non-overset surface topologies for the baseline fuselage+hub configuration. The overset boundaries are created in the second step. Figure 4 shows the overset boundary placement. These boundaries are used for all hub configurations in this study. Finally, the rotating and non-rotating components are separated into different ICEM project files to begin surface mesh generation. Figure 5 shows the surface mesh of the baseline overset clean hub mesh.

After surface mesh generation, volume mesh generation follows as described above. The overset boundaries are treated like the farfield boundary and are set to no prismatic growth. The volume enclosed by the overset boundary in the fuselage mesh is not filled with grid points. This is done to reduce the total grid size, minimize computational overhead, and to simplify the overset topology for SUGGAR++.

Figure 6 is a cut plane that shows the overset grid topology and connectivity for an isolated rotating hub configuration.

Once volume mesh generation is completed, the component grids are assembled into a composite overset mesh with SUGGAR++. A donor quality of 0.9 is specified and anywhere from 0-2 orphans were created in the overset assembly. Orphan points were found to be deep inside the hub well region and not to affect the solution. If orphan points were found outside of this region, the components grids and their overset boundaries would have to be regenerated to fix the issue. Orphans were either eliminated by moving the overset boundaries or changing the surface resolution on the boundaries. However, once an acceptable overset boundary configuration was found, it was used for all subsequent hub configurations. The ability to reuse the overset boundary surfaces significantly reduced the grid generation time for the faired hub configurations discussed below.

Hub Fairing Design and Grid Generation

In addition to the wind tunnel model hub geometry, different hub fairing geometries were experimented with computationally. Three fairing geometries were examined: a large hub fairing (HF), a slim hub fairing (SF), and a "beanie"-style fairing. The large hub is shown in Figure 7. It has a pseudo-ellipsoid cross-section (it is actually an amalgamation of two parabolas using cubic splines, and thus not a true ellipse) with a 20% thickness-to-chord ratio and extends to 15% of a full rotor radius. The thickness and chord length were selected based on the study by Martin et al. [Ref . 18]. The slimmed hub fairing is shown in Figure 8. It has an elliptic cross-section with a thickness-to-chord ratio of 33.3%, where the chord and the thickness are the major and minor axis lengths of the ellipse, respectively. The fairings are extended smoothly to the blade stubs by scaling down the ellipse cross-section. The cross-section remains constant from the edge of the blade grips to the center of the hub. The beanie fairing is shown in Figure 9. It is created as body of revolution using a circular arc. It has a thickness-to-chord ratio of 16%.

Separate component grids were generated for each hub fairing design using ICEM. Each is interchangeable with the original hub component mesh. All simulations used the same fuselage and background mesh.

COMPUTATIONAL RESULTS

Static Hub Results

Before initiating the rotating hub calculations, the overset hub model was first run statically to drive out any startup transients and to provide an "apples-to-apples" comparison for static versus rotating hub configurations. All steady simulations had the blades indexed at 45°. Each case achieved convergence in 2000 iterations. Depending on the size of the mesh and the number of cores used (anywhere from 36 to 60), computation time varied between two and eight hours. Additionally, runs were conducted with the fuselage with the hub well for comparison with the clean fuselage runs. The drag, lift, and pitching moment results from this pitch sweep are shown in Figure 10. The difference in drag between the two fuselage geometries is less than 5%.

The drag, lift, and pitching moment results from the pitch sweep are shown in Figure 11 and the lift vs. drag curves are shown in Figure 12. Hub drag has been defined as the difference between the zero-lift drag values of the fuselage and hub configurations and the fuselage only configuration (Ref. 4-5). Using this definition, the FUN3D computations under predict the hub drag by 13%. However, it is important to note here that in the wind tunnel data the zero-lift angle of attack for the fuselage alone configuration is significantly different than the zero-lift angle of attack for the fuselage and hub configuration (the same is true for the computations, but the gap is much smaller). It was also found that the minimum drag location predicted by FUN3D is much closer to the wind tunnel result than the previously reported U^2NCLE results by Bridgeman, as shown in Figure 13. If the hub drag is instead defined to be the difference between the drag values of the fuselage and hub configuration and the fuselage alone configuration at zero angle of attack, the computations under predict the hub drag by less than 7%.

The drag, lift, and yawing moment results from the yaw sweep are shown in Figure 14. The side force vs. yaw angle and drag curves are shown in Figure 15. The computational results for the drag, side force, and yawing moment are all in good agreement with the experimental results. In fact, if the hub drag is defined to be the difference between the drag values of the fuselage and hub configuration and the fuselage alone configuration at zero yaw angle, the computations match the experiment nearly perfectly (0.1% difference).

The three fairings that were tested gave results ranging from substantial hub drag reduction to slight hub drag addition. Steady runs were conducted at

zero angle of attack and zero yaw angle with each configuration. The total model drag for each configuration is shown in Figure 16. The data are normalized by the baseline (no fairing) configuration and broken down into the two components, the fuselage and the hub. The large hub fairing (HF) and the slim hub fairing (SF) offer drag reductions of 10% and 20% of the total model drag, respectively. The beanie fairing (BF) resulted in a 6% increase in total model drag. The drag on the entire model is compared instead of just the hub component because the fuselage component drag is also affected by the fairings due to interference effects (i.e. the changes in the hub wake and the flow field that the tail boom encounters). The fuselage component drag varies between the fairing configurations over a range of 6% of the total model drag. In fact, two-thirds of the drag addition from the beanie fairing is realized in the fuselage component drag. This demonstrates the importance of testing these hub drag reduction concepts with the fuselage present.

Rotating Hub Results

Due to computational resource constraints, a reduced selection of pitch and yaw runs were made of the rotating hub simulations. All rotating hub cases were initialized from the corresponding static hub solution.

The time step was selected based on the hub rotation speed and the characteristic period (1 quarter hub rotation) of the simulation. 400 time steps per hub rotation were used with a max subiteration count of 50. The temporal error controller was also used to reduce the number of subiterations. All rotating hub simulations were run for three revolutions or 1200 time steps. It was found that the results became periodic after the first revolution, as shown in Figure 17. The rotating cases took about four days to run on 60 cores.

The results shown in Figures 14 and 15 are averaged over two revolutions. As can be seen in Figures 2, 14, and 15, there is little difference between the static and rotating hub drag results in both the wind tunnel results and the computational results.

As with the baseline (no hub fairing) results, little change in drag is seen between the static and rotating hub cases for the different fairing configurations. The total model drag for each of the configurations, static and rotating, is shown in Figure 18. The data are normalized by the static baseline configuration. The change between the static and rotating drag for any of the fairing configurations is less than 2% of the total baseline model drag.

The static and rotating velocity fields for the baseline case and the three hub fairings are shown in Figures 19-22. It is clear that the computations are capturing the differences in the flowfield while still coming to the same conclusion as the wind tunnel tests: rotating the hub, in this case, does not change the drag results.

CONCLUSIONS AND FUTURE WORK

The experimental and computational results obtained during the final year of our NRTC/VLC project have been reported. The wind tunnel data set was from a current generation Bell Helicopter aircraft. The model build up resulted in measured data on an isolated fuselage and a fuselage and hub configuration. Measurements were made both as the hub remained fixed and as it rotated.

Using the methods developed in this project, good correlation was found with experimental results. First of all, computational results were found to be within 10% of experiment using a clean hub (no fasteners) geometry. Secondly, the computational results agree with experiment in that the drag does not change when the hub is rotating versus when it is stationary. This result shows that rotating hub simulations are unnecessary to make accurate drag predictions. This is a significant benefit since a static case can be run for a fraction of the computational cost of a rotating hub simulation. Additionally, a computational experiment was carried out to investigate the benefit of different hub fairing geometries. A drag benefit of up to 20% was found with the slim hub fairing over baseline configuration.

In the immediate future a grid resolution study needs to be conducted using the present computational method in order to ensure that it is being operated at the highest (realistically) obtainable accuracy. A detailed hub (including fasteners) model also needs to be run. The grids used herein were based on the resolution settings developed for the U^2NCLE solver by Bridgeman and a similar study needs to be performed for FUN3D. Additionally, a temporal resolution study is needed for the rotating hub case in order to determine the optimal number of time steps needed per revolution. The unsteady methodology will also be validated against PIV data of the hub wake region generated during the the wind tunnel test (not reported here). Unsteady flow interactions between the hub wake and tail are still poorly understood, and accurate and efficient rotating hub computations are needed to investigate (and predict) the interactional aerodynamics.

ACKNOWLEGMENTS

This project was funded by the Vertical Lift Consortium (VLC), formerly the Center for Rotorcraft Innovation and the National Rotorcraft Technology Center (NRTC), U.S. Army Aviation and Missile Research, Development and Engineering Center (AMRDEC) under Technology Investment Agreement W911W6-06-2-0002, entitled National Rotorcraft Technology Center Research Program. The authors would like to acknowledge that this research and development was accomplished with the support and guidance of the NRTC and VLC. The views and conclusions contained in this document are those of the authors and should not be interpreted as representing the official policies, either expressed or implied, of the AMRDEC or the U.S. Government. The U.S. Government is authorized to reproduce and distribute reprints for Government purposes notwithstanding any copyright notation thereon.

REFERENCES

1. Gormont, R.E., "Some Important Practical Design Constraints Affecting Drag Reduction," Rotorcraft Parasite Drag Special Report, presented at the 31st Annual Forum of the American Helicopter Society, Washington, D.C., May 14–15, 1975.
2. Sheng, C., Wang, X., "Characteristic Variable Boundary Conditions for Arbitrary Mach Number Algorithm in Rotating Frame," AIAA Paper 2003-3076, June 2003.
3. Sheng, C., Wang, X., and Narramore, J., "Computational Simulation Analysis of a Quad Tilt-Rotor Aero Interaction Using a Navier-Stokes Solver," 64th Annual Forum of the American Helicopter Society, Montreal, Canada, April 2008.
4. Bridgeman, J.O., and Lancaster, G.T., "Predicting Hub Drag on Realistic Geometries," presented at the 2010 AHS Specialist's Meeting on Aeromechanics, San Francisco, CA, January 20–22, 2010.
5. Bridgeman, J.O., and Lancaster, G. T., "Physics-Based Analysis Methodology for Hub Drag Prediction," presented at the 66th Annual Forum of the American Helicopter Society, Phoenix, AZ, May 2010.
6. Anderson, W.K. and Bonhaus, D.L., "An Implicit Upwind Algorithm for Computing Turbulent Flows on Unstructured Grids," *Computers and Fluids*, Vol. 23, (1), 1994, pp. 1-22.
7. Biedron, Robert T., Thomas, James L., "Recent Enhancements to the FUN3D Flow Solver for Moving Mesh Applications," AIAA Paper 2009–1360.
8. Noack, R. W., "DiRTlib: A Library to Add an Overset Capability to Your Flow Solver," AIAA Paper 2005-5116, June 2005.
9. Noack, R. W., Boger, D. A., Kunz, R. F., and Carrica, P.M., "SUGGAR++: An Improved General Overset Grid Assembly Capability," AIAA Paper 2009-3992, June 2009.
10. Young, L.A, Graham, D.R., Stroub, R.H., Louie, A.W., "Reduction of Hub and Pylon-Fairing Drag," American Helicopter Society, 43rd Annual Forum Saint Louis, MO, May 1987.
11. Young, L.A. and Graham, D.R., "Experimental Investigation of Rotorcraft Hub and Shaft Fairing Drag Reduction," 4th AIAA Applied Aerodynamics Conference, San Diego, CA, June 1986.
12. Stroub, R.H., Young, L.A., Louie, A.W., "Investigation of Generic Hub Faring and Pylon Shapes to Reduce Hub Drag," 13th European Rotorcraft Forum, Arles, France, September 1987.
13. Stroub, R.H., Young, L.A., Louie, A.W., "Investigation of Generic Hub Fairing and Pylon Shapes to Reduce Hub Drag," NASA TM 100008, September 1987.
14. Young, L.A., Graham, D.R., and Stroub, R.H., "Experimental Investigation of Rotorcraft Hub and Shaft Fairing Drag Reduction," *AIAA Journal of Aircraft*, Vol. 24, Dec. 1987, p. 861-867.
15. Graham, D.R., Sung, D.Y., Young, L.A., Louie, A.W., and Stroub, R.H., "Helicopter Hub Fairing and Pylon Interference Drag," NASA TM 101052, January 1989.
16. Sung, D.Y., Lance, M.B., Young, L.A., and Stroub, R.H., "An Experimental Investigation of Helicopter Rotor Hub Fairing Drag Characteristics," NASA TM 102182, September 1989.
17. Martin, D.M., Mort, R.W., Squires, P.K., and Young, L.A., "Hub and Pylon Fairing Integration for Helicopter Drag Reduction," 47th Annual Forum of American Helicopter Society, Phoenix, AZ, May 6–8, 1991.
18. Martin, D.M., Mort, R.W., Young, L.A., and Squires, P.K., "Experimental Investigation of Advanced Hub and Pylon Fairing Configurations to Reduce Helicopter Drag," NASA TM 4540, September 1993.
19. Wake, B.E., Hagen, E., Ochs, S.S., Matalanis, C.G., and Scott, M.W., "Assessment of Helicopter Hub Drag Prediction with an

Unstructured Flow Solver," American Helicopter Society 65th Annual Forum, Grapevine, Texas, May 2009.
20. Le Chuiton, F., Kneisch, T., Schneider, S., and Krämer, Ph., "Industrial Validation of Numerical Aerodynamics About Rotor Heads: Towards a Design Optimisation at Eurocopter," presented at the 35th European Rotorcraft Forum, Hamburg, Germany, September 2009.
21. Shenoy, R., Holmes, M., Smith, M.J., Komerath, N. M., "Computational Investigation of Hub Drag Reconstruction from Model to Full Scale," presented at the 37th European Rotorcraft Forum, Milan, Italy, September 2011.
22. Spalart, P.R., Allmaras, S.R., "A One-Equation Turbulence Model for Aerodynamic Flows," AIAA Paper 92-0439, January 1992.
23. Vatsa, V., Carpenter, M.H., "Higher-Order Temporal Schemes with Error Controllers for Unsteady Navier-Stokes Equations," AIAA Paper 2005-5245, June 2005.
24. Vatsa, V., Carpenter, M.H., Lockard, D.P., "Reevalutation of an Optimized Second Order Backward Difference (BDF2OPT) Scheme for Unsteay Flow Applications," AIAA Paper 2010-0122, January 2010.
25. SAS IP, Inc., ANSYS ICEM CFD User's Manual, version 13.0, 2010.
26. Gaither, J.A., Marcum, D. L., Mitchell, B.,"SolidMesh: A Solid Modeling Approach to Unstructured Grid Generation." 7th International Conference on Numerical Grid Generation in Computational Field Simulations, Whistler, B.C., Sept. 2000.
27. Marcum, D.L., Gaither, J.A., "Unstructured Surface Grid Generation Using Global Mapping and Physical Space Approximation," 8th International Meshing Roundtable, South Lake Tahoe, CA, Oct. 1999.
28. Marcum, D.L. Gaither, J.A., "Mixed Element Types Unstructured Grid Generation for Viscous Flow," AIAA Paper 99-325A, 1999.

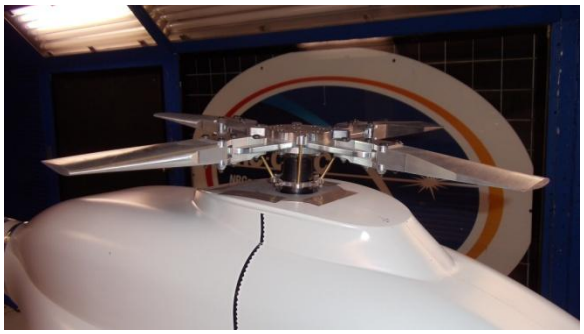

Figure 1. Rotating hub wind tunnel model.

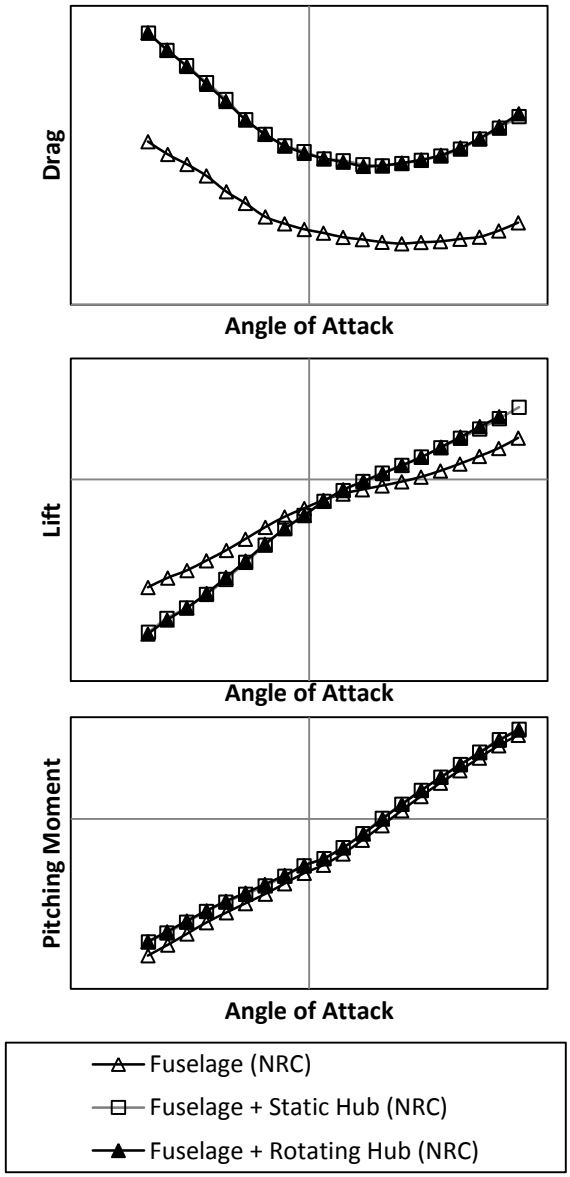

Figure 2. Wind tunnel results for drag, lift, and pitching moment vs. angle of attack.

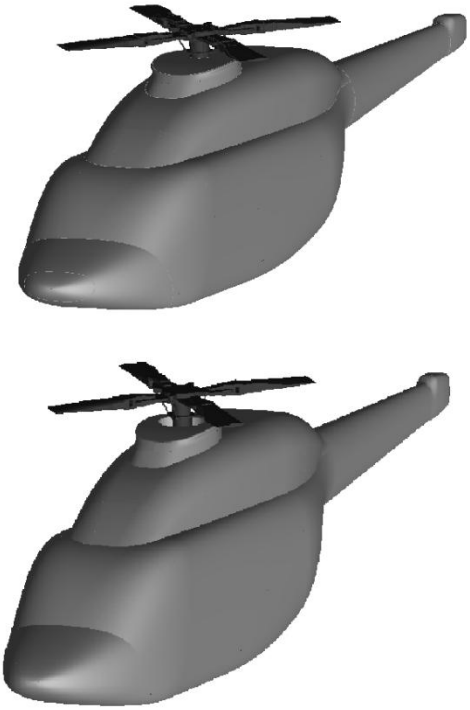

Figure 3. Comparison of non-overset (top) and overset (bottom) surface models.

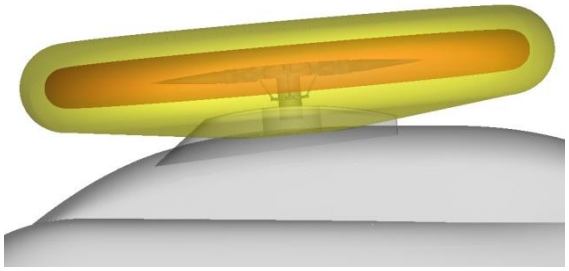

Figure 4. Overset boundary placement.

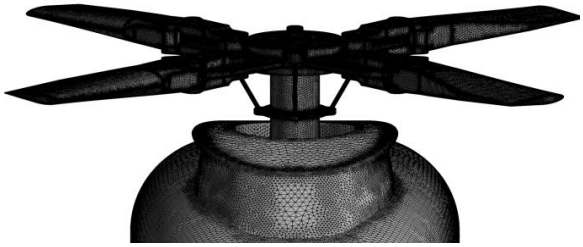

Figure 5. Overset hub surface mesh topology.

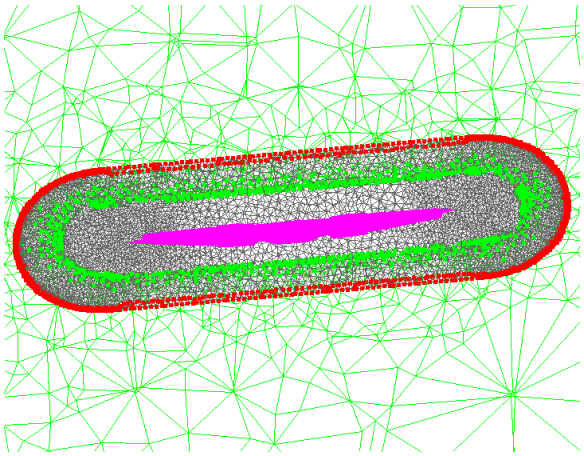

Figure 6. Overset grid domain connectivity.

Figure 7. Large hub fairing geometry. (HF)

Figure 8. Slim hub fairing geometry. (SF)

Figure 9. Beanie fairing geometry. (BH)

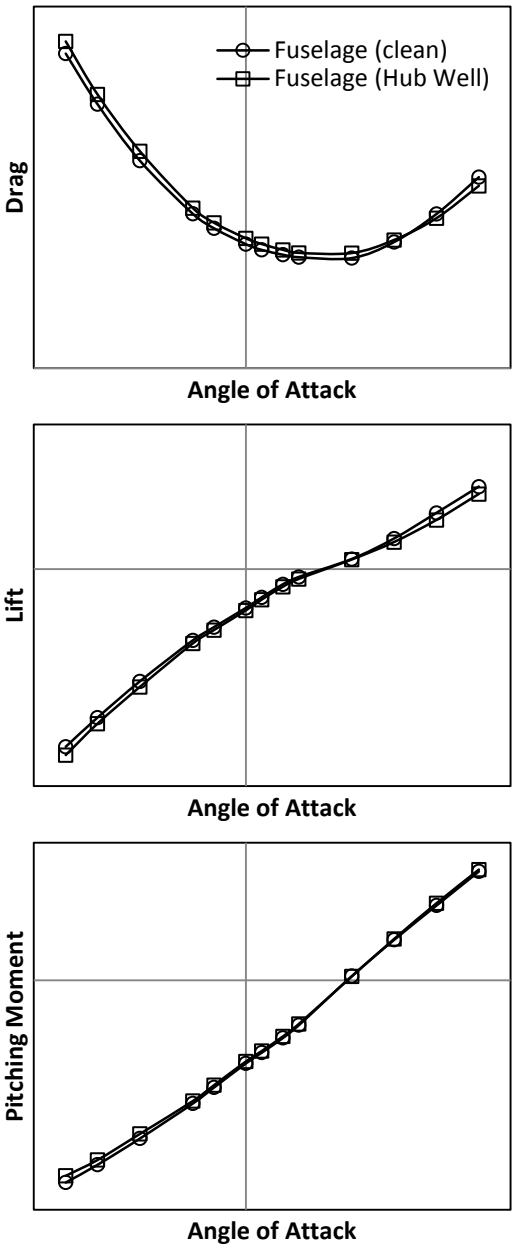

Figure 10. Drag, lift, and pitching moment vs. angle of attack, clean fuselage and fuselage with hub well comparison.

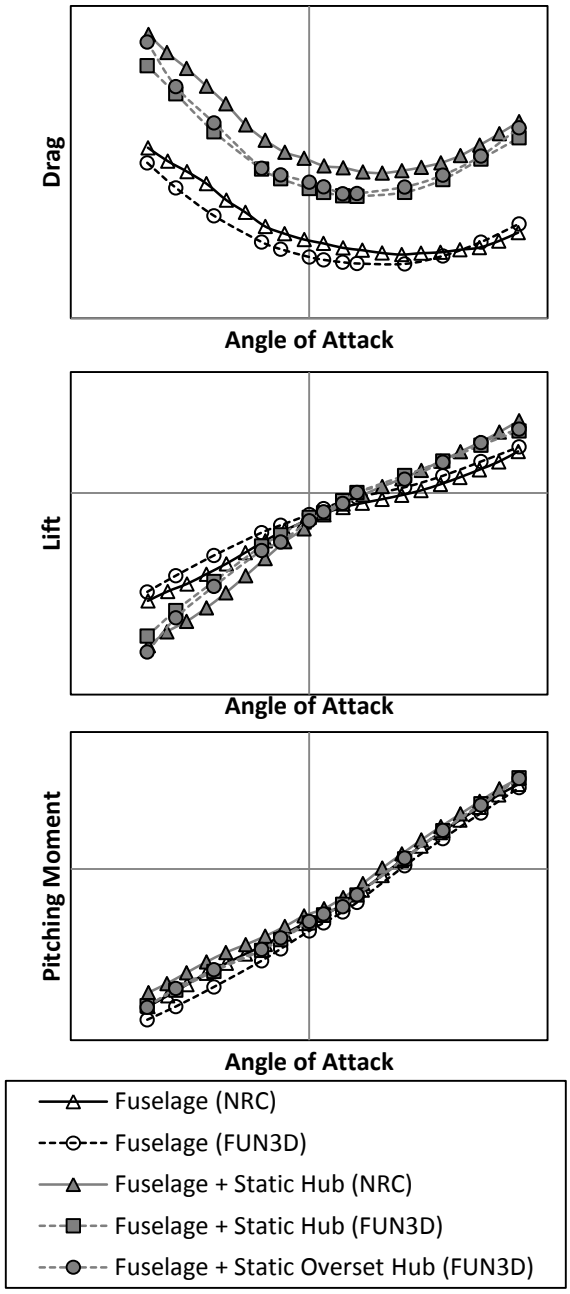

Figure 11. Drag, lift, and pitching moment vs. angle of attack.

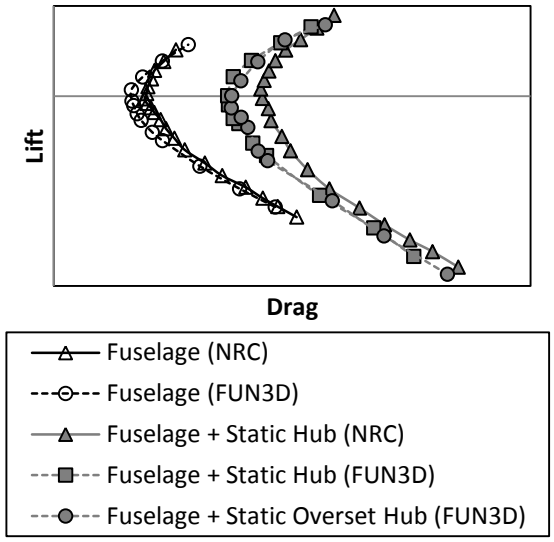

Figure 12. Lift vs. drag curves from pitch sweep.

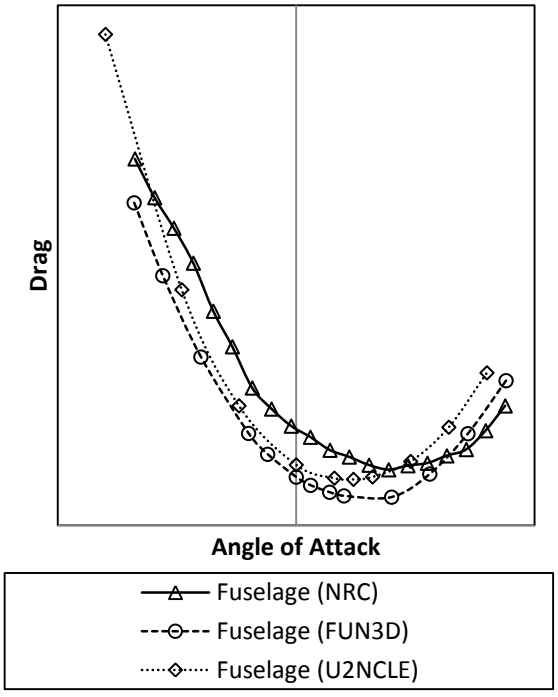

Figure 13. Drag vs. angle of attack curves, clean fuselage.

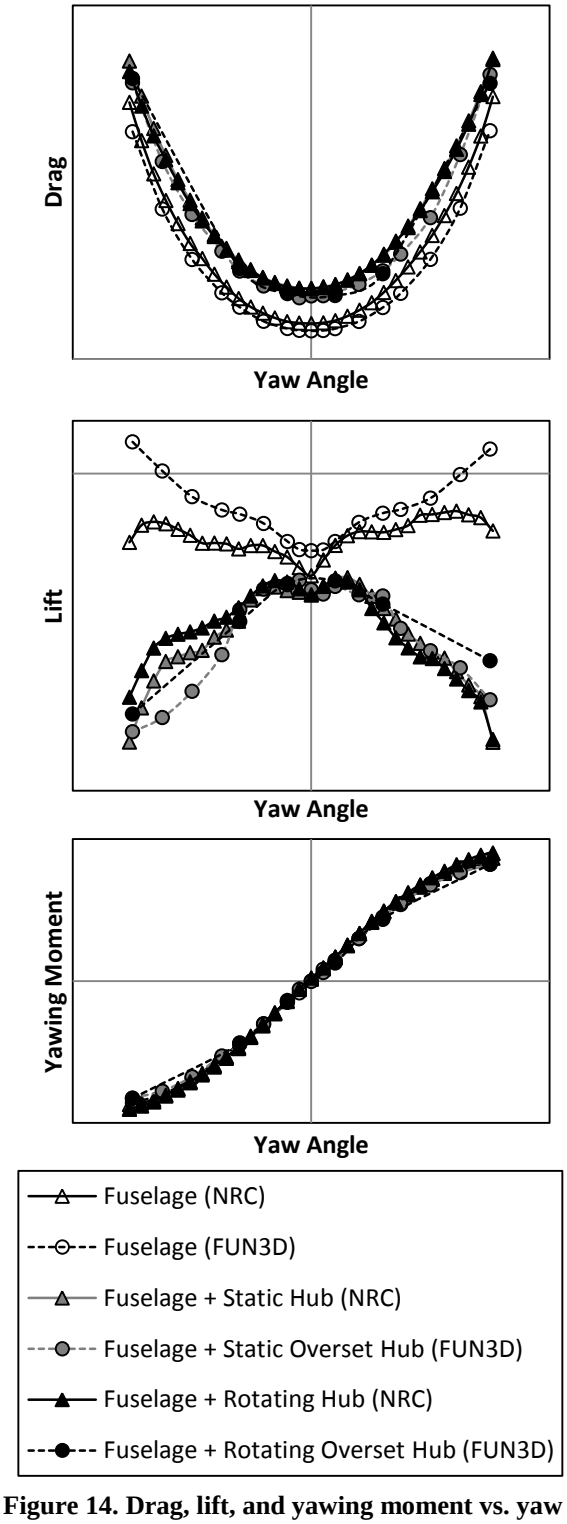

Figure 14. Drag, lift, and yawing moment vs. yaw angle.

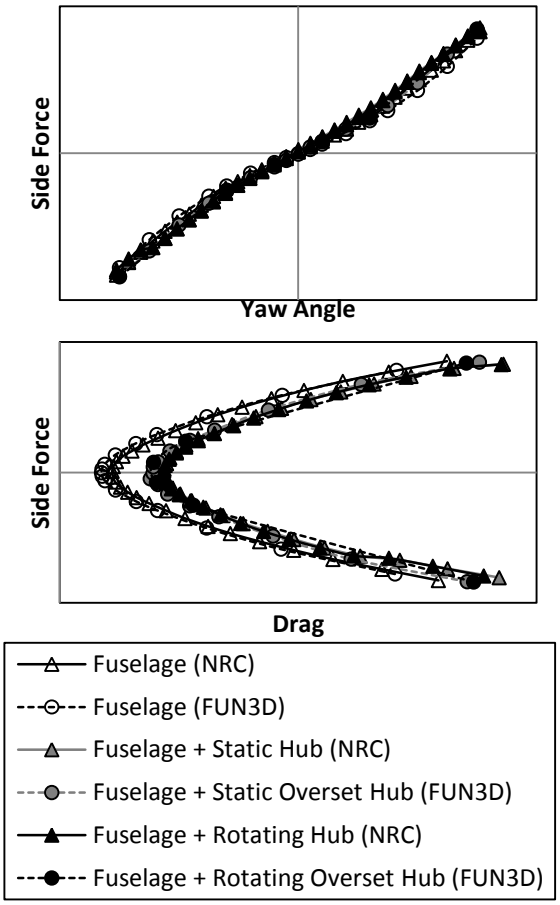

Figure 15. Side force vs. yaw angle and drag, from yaw sweep.

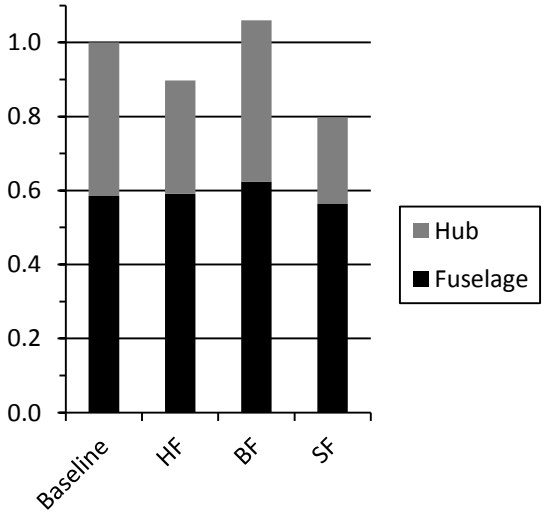

Figure 16. Drag comparisons, static hub with fairings.

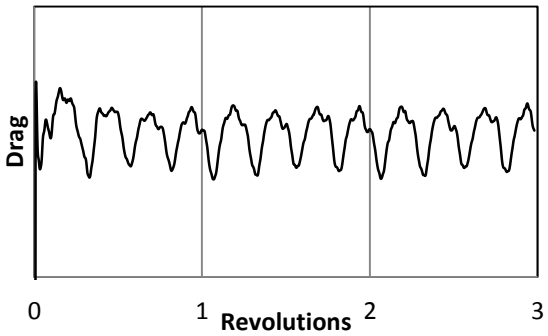

Figure 17. Time history of CFD predicted drag for baseline rotating hub case.

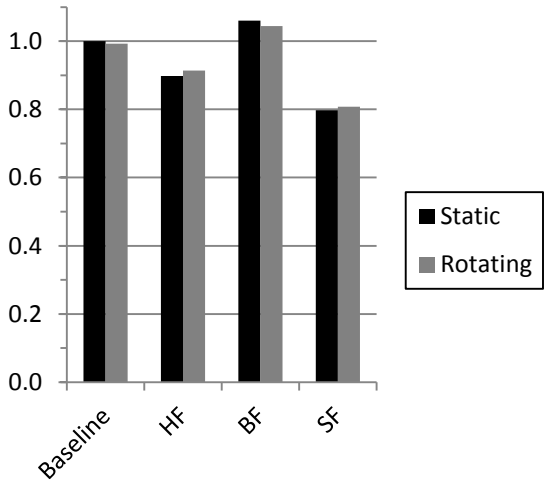

Figure 18. Drag comparisons, static and rotating hub with fairings.

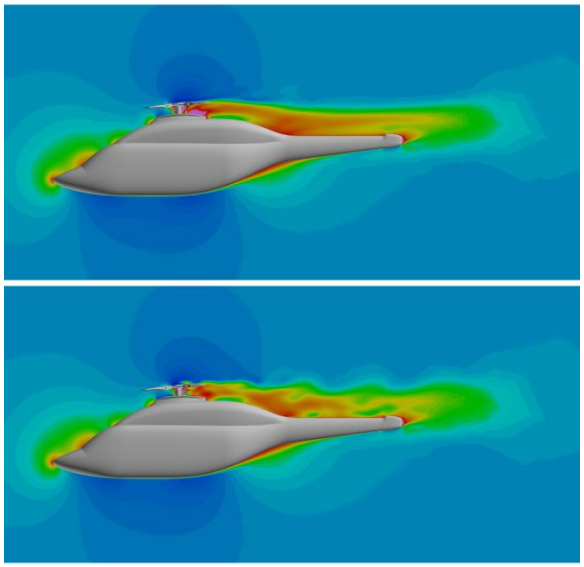

Figure 19. Static (top) and rotating (bottom) streamwise velocity contours, wind tunnel geometry.

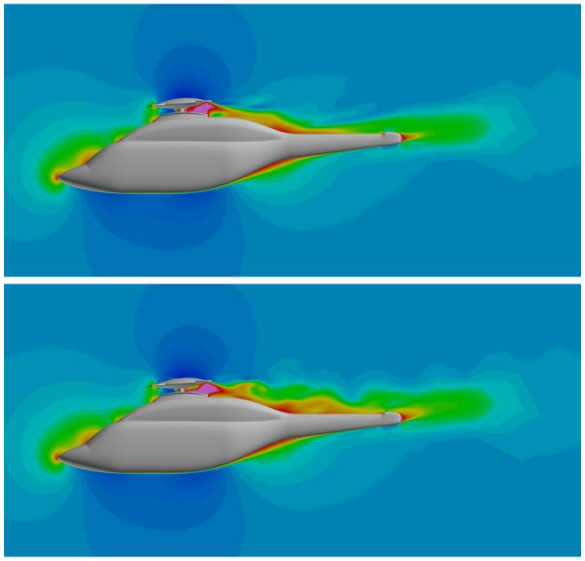

Figure 20. Static (top) and rotating (bottom) streamwise velocity contours, large hub fairing geometry.

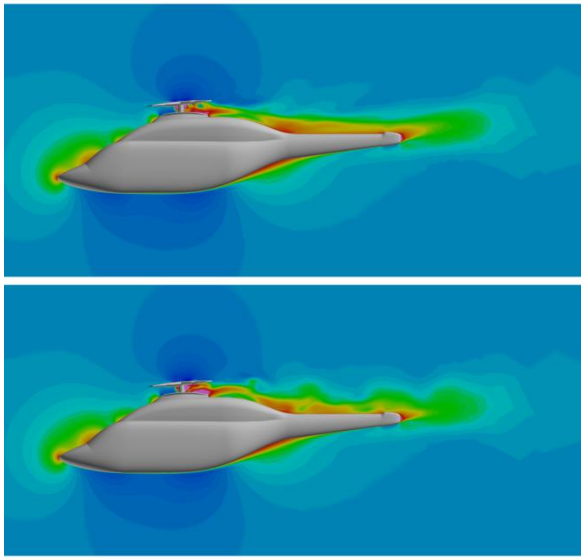

Figure 21. Static (top) and rotating (bottom) streamwise velocity contours, slim hub fairing geometry.

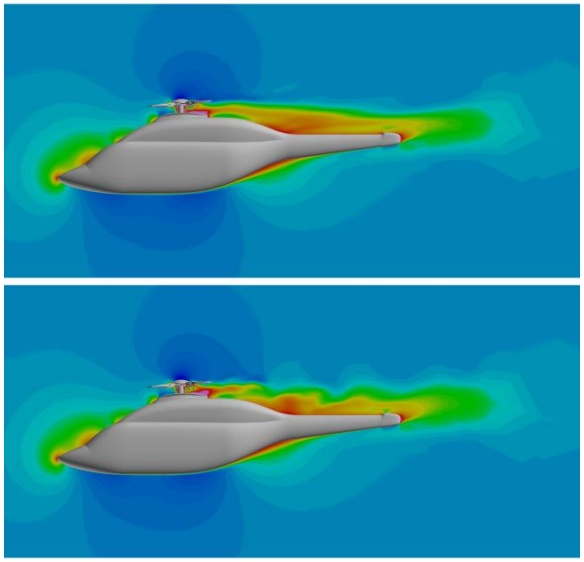

Figure 22. Static (top) and rotating (bottom) streamwise velocity contours, beanie fairing geometry.